

Subwavelength Transmission Gratings and Their Applications in VCSELs

Stephen Y. Chou^{a,b}, Steve Schablitsky^b, and Lei Zhuang^{a,b}

^aNanoStructure Laboratory, Department of Electrical Engineering
Princeton University, Princeton, NJ 08544

^bDepartment of Electrical and Computer Engineering
University of Minnesota, Minneapolis, MN 55455

ABSTRACTS

Birefringence, polarization, and wavelength filtering properties of subwavelength transmission gratings (SWTGs) and their applications in vertical cavity surface emitting lasers (VCSELs) are presented. Particularly, large birefringence (over two orders of magnitude larger than natural birefringence crystals) and polarization effects have been achieved in thin (240 nm thick or less) amorphous silicon subwavelength gratings (SWTGs). The SWTG polarizers were used to control the polarization of VCSELs (i.e., fixing, enhancing and switching of the polarization), making the maximum polarization of a VCSEL creased to 300:1 from 20:1. The SWTG's waveplates were used to build a polarization-switching VCSEL oscillator that has a can tunable frequency up to terahertz.

Keywords: subwavelength, gratings, lasers, birefringence, polarization, band filter, high frequency pulse, nanoimprint lithography, electron beam lithography

1. INTRODUCTION

Subwavelength transmission gratings (SWTGs) are the gratings with a period less the wavelength of light and no non-zero order diffraction. Depending upon their materials and dimensions, SWTGs can function as waveplates, polarizers, narrow wavelength filters, antireflection coating, or phase modulators. One unique advantage of SWTGs (as well as other subwavelength optical elements) is that their thickness can be merely a fraction of a wavelength (e.g. 250 nm thick), rather than millimeters as required in conventional bulk optical elements. Another unique advantage is that SWTGs are made of amorphous materials and can be monolithically fabricated anywhere on a wafer. The first properties makes SWTGs suitable for high speed applications where the cavity length is a limiting factor. The second property makes SWTGs suitable for large area integrated optics, which are a key to future telecommunications and integrated circuit interconnections.

Despite their promises, SWTGs were studied primarily by simulation (except form birefringence) and were never seriously considered for practical application because of the difficulty and the high cost involved in their fabrication. However, nanoimprint lithography, invented recently, offers a low cost, high throughput, reliable means to fabricate SWTGs, hence opening up great opportunities for the investigation and application of SWTGs.

Email: chou@ee.princeton.edu

SWTGs are naturally suited for integration with vertical cavity surface emitting lasers (VCSELs). Such integration can lead to many unique functions, such as (a) fixing, enhancing and switching a VCSEL's polarization, (b) making the VCSEL's modes oscillating between two polarization modes at a high frequency (up to THz and tunable), and (c) selecting the wavelength of a VCSEL. In this paper, we will review our work on SWTGs and application in VCSELs[1-3].

2. SUBWAVELENGTH TRANSMISSION GRATINGS

The behavior of a subwavelength transmission gratings depends upon the refractive index of the grating and the surrounding materials, as well as the ratio of grating period to the wavelength of light. Here, we will discuss, from the experimental point of view, three properties of a SWTG: birefringence, polarization, and wavelength filtering.

2.A Form Birefringence Regime

A large birefringence can be achieved in a SWTG when the period of the grating is much smaller than the wavelength of the light. In this regime, the grating can be treated as a layer of homogeneous medium, but having different refractive indices for the TE wave (the electric vector parallel to the grating grooves), n_{TE} , and the TM waves (the electric vector normal to the grating grooves), n_{TM} . The difference in the index comes from the difference in boundary conditions: for TE wave, E field is continuous but not D field; for TM waves, D field is continuous but not E field. Therefore the effective dielectric constants are [4]

$$\begin{aligned} \text{for TE wave,} \quad \epsilon_{\parallel} &= f\epsilon_1 + (1-f)\epsilon_2 \\ \text{for TM wave,} \quad \epsilon_{\perp} &= \frac{\epsilon_1\epsilon_2}{f\epsilon_2 + (1-f)\epsilon_1} \end{aligned}$$

where ϵ_1 is the dielectric constant of the grating material, ϵ_2 is the dielectric constant of the filling material, and f is the ratio of the grating width to period.

From rigorous modal expansion theory (RMET), the form birefringence regime corresponds to the case where only one eigen mode exists inside the SWTGs [5].

The form birefringence, Δn , is usually much larger than that of the conventional uniaxial materials used for waveplate applications. For examples, Δn for mica and quartz are 0.005 and 0.009, respectively. But, for silicon, Δn is 1.2, which is more than two orders of magnitude larger, implying that the thickness of a waveplate can be more than two orders of magnitude thinner.

2.B Polarization Regime

As the period of a SWTGs becomes larger, more than one eigen mode can exist inside the SWTGs, while no non-zero order diffraction exists outside. In this case, TE and TM waves will couple differently into these eigen modes, which will further interact differently at the grating surfaces, leading to drastically

different transmissions (hence polarization effect). RMET analysis has showed that the transmission ratio for the two waves can become infinite [5].

2.C. Narrow Band Filtering

Further RMET analysis showed that in the polarization regimes, not only do the TE and TM wave have different transmission, but also the transmission of each wave is very sensitive to the wavelength of the incident light. For a given grating period, the transmission (hence the reflectance) vs. The wavelength has a full peak width at half maximum as narrow as a fraction of a nanometer[6,7]. Therefore, it offers an excellent narrow band filter. The sharp peak is due to the resonance in a grating waveguide.

2.D Experimental Results

We have fabricated amorphous Si (α -Si) SWTG on fused silica substrates (Fig. 1 and 2)[1-3]. The SWTG has a period ranging from 100 nm to 800 nm and the thickness is 180 nm and 250 nm. The experimental and theoretical transmittance of TE and TM waves (633 nm wavelength) through the 180 nm thick gratings (Fig. 3) showed strong dependence on the grating period. The phase difference between transmitted TE and TM waves is also a strong function of the grating period (Fig. 4). When the grating period is less than 0.4λ , the SWTGs have almost the same transmittance for TE and TM waves but very difference phase, acting like a waveplate. However, when the grating period is between 0.4λ and 0.8λ , SWTGs have very different transmittance for the two waves, acting like a polarizer.

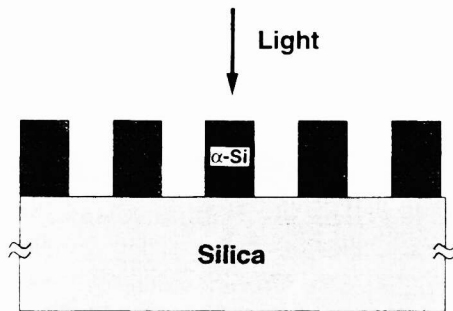


Fig. 1. Schematic of a thin subwavelength transmission grating.



Fig. 2. Amorphous silicon gratings with 100 nm period and 240 nm thickness on silica.

The experimental and theoretical reflectance of α -Si SWTGs (240 nm thick) for $\lambda=850$ nm light is also a strong function of the grating period (Fig. 5). The TM wave has a maximum reflection at the grating period around 0.4λ , while the TE wave has a minimum reflection at the period about 0.5λ . Since the sum of the measured reflectivity and transmittivity is close to unity (except for periods larger than 600 nm), the absorption of the gratings is negligible, which is a result of the large effective band gap of the amorphous Si and the small thickness. For periods larger than 600 nm, diffraction effects from the gratings become significant and cause losses in the total transmitted and reflected light, leading to a difference in the experimental data and simulation. For periods smaller than 400 nm, the experimental data also deviates from

the theoretical simulation. The discrepancy may be due to the fact that the simulation assumes the gratings to have a square shape, while the actual grating shape for these small periods is a sine wave.

It should be pointed out that subwavelength dielectric grating wave plates made of low refractive index materials such as photoresist [8], quartz [9], PMMA, and silicon nitride [10] have been previously fabricated. Their low reflective index requires a thickness larger than α -Si SWTGs for the same phase retardation.

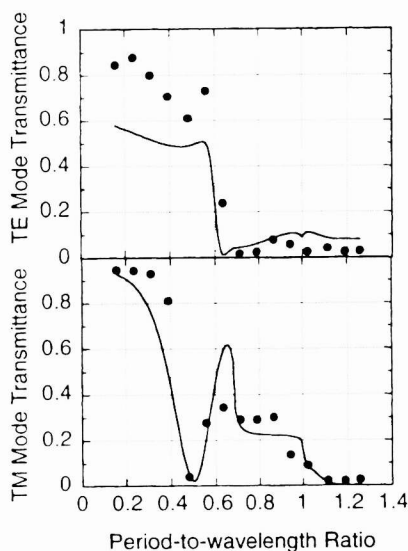


Fig. 3. Measured (dots) and simulated (solid line from RMET) transmittance of TE and TM waves ($\lambda = 677$ nm) through a 180 nm thick α -Si grating.

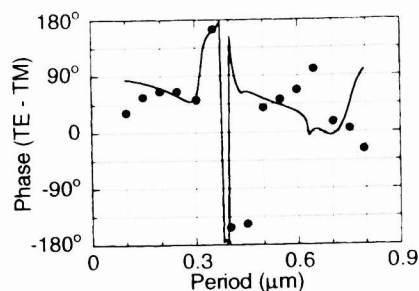


Fig. 4. Measured (dots) and simulated (solid lines) phase retardation between TE and TM waves ($\lambda = 677$ nm) through a 180 nm thick α -Si grating.

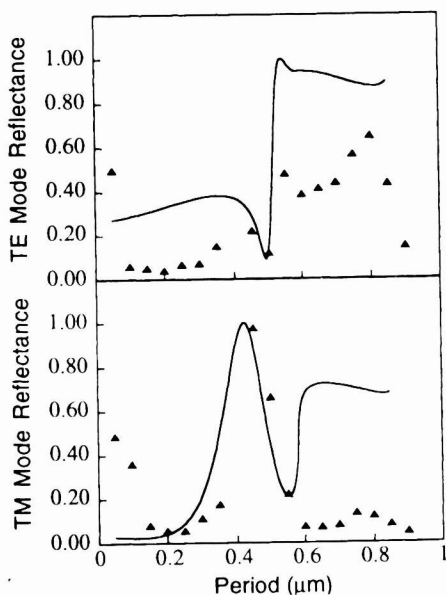


Fig. 5. Measured (dots) and simulated (solid lines) reflectance of TE and TM waves ($\lambda = 850$ nm) of the SWTGs of 250 nm thick.

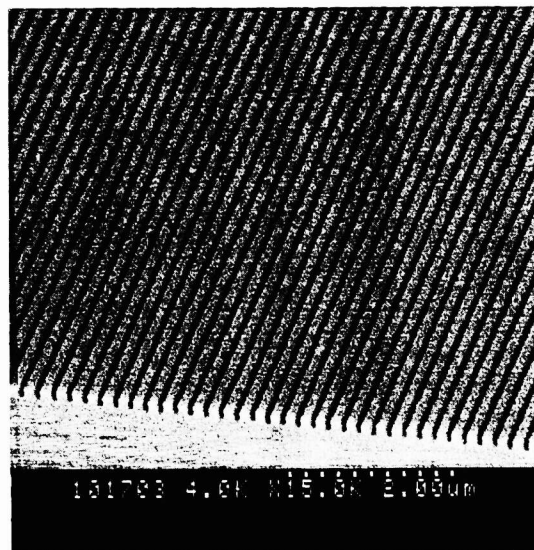


Fig. 6. SiO_2 gratings with 180 nm period and 250 nm thick fabricated using nanoimprint lithography and RIE.

2. FABRICATIONS AND NANOIMPRINT LITHOGRAPHY

Fabrication of SWTGs is based on microfabrication technology. It starts with depositing a thin layer materials on a substrate, followed by patterning the material with lithography and etching. Due to the subwavelength feature size, the lithography must have a sub-200 nm resolution. Typically, electron beam lithography is used, although x-ray, ion beam, or scanning probe lithography are also applicable. However, the conventional high resolution lithographies are very expensive, not readily available, and usually have a low throughput. This poses a serious roadblock for the study and application of SWTGs.

Nanoimprint lithography, invented recently, can produce sub-10 nm feature size over a large area with a high throughput and low cost--a feat that is impossible with current conventional lithography[11]. Nanoimprint lithography patterns a resist by deforming the resist shape through embossing (with a mold), rather than by altering resist chemical structures through radiation (with particle beams). After the embossing resist, an anisotropic etching is used to remove the residue resist in the compressed area to expose the underneath substrate. Uniform SiO₂ gratings of 180 nm period over a 5 cm by 5 cm area have been fabricated using nanoimprint lithography (Fig. 6) [12].

3. CONTROLLING THE POLARIZATION OF VCSELS

The output light of VCSELS have two linearly polarized modes orthogonal to each other: along the $\langle 011 \rangle$ and $\langle 01\bar{1} \rangle$ crystal direction, denoted as P_{||} and P_⊥ respectively[13]. Under normal operation, one of the modes will dominate over the other, with a typical polarization ratio of 10:1. However, the two modes, due to the nearly equal gain, are not stable and can be switched from the strong to the weak and vice versa, when device operating parameters vary (e.g. injection current). Efforts have been made to control the polarization by using anisotropic transverse cavity geometry [14,15], induced active layer stress from an elliptical window [16], asymmetrically designed active layers [17], and metal gratings on the bottom reflector of the VCSEL [18]. However, these methods all involve a direct alteration of the laser cavity, making it difficult to obtain uniformity and simplicity in processing. It is more desirable to obtain polarization control without significantly changing the cavity structure.

Placing a SWTG polarizer in front of the VCSEL output window offers an effective way to control the polarization (such as locking, enhancing, and switching of the modes)[2]. A SWTG polarizer, which is only a fraction of wavelength thick, will reflect one mode back into the laser cavity more favorably than the other mode, forcing the lasing polarization to be locked in the mode reflected favorably. If the favored reflected mode is a strong mode, then the strong mode becomes stronger while the weak mode becomes weaker, enhancing the laser polarization. If the favored reflected mode is a weak mode, then the weak mode becomes the strong mode while the initial strong mode switches to a weak mode.

From the reflectivity shown in Fig. 5, the α -Si SWTG with a period of 100 nm (240 nm thick) seems to have the best characteristics for polarization locking. Namely, it has a very low TE mode reflectance (5%) but a decent TM mode reflectance (35%). To produce optical feedback for polarization locking, the output light from the VCSEL is collimated into a parallel beam using an objective lens. Because of the small grating area, another objective lens is used to focus the beam onto the SWTG to a spot having a diameter of 10 μ m.

The laser spot and SWTG are monitored by an optical microscope and camera through a beam splitter. However, during measurements the beam splitter was removed to reduce birefringence. The light transmitted through the SWTG is again collimated and analyzed using a linear polarizer and a photodetector.

Figure 7(a) shows the output light power of the VCSEL (a commercial one by VIXEL Co.) vs. injection current for the P_{\parallel} and P_{\perp} modes without a SWTG. The VCSEL has a threshold current of 9 mA, and P_{\parallel} is the strong mode. Fig. 7(b) shows the output power for the P_{\parallel} and P_{\perp} modes with the 100 nm period SWTG placed in front of the VCSEL's output window and the grating fingers parallel to the P_{\parallel} direction. As pointed out before, in this orientation light from the P_{\perp} mode is more favorably reflected back to the cavity, therefore the P_{\perp} mode is switched from the weak mode to the strong mode, and the P_{\parallel} mode becomes nearly zero. Fig. 7(c) shows the output power when the SWTG is rotated 90° so that the grating fingers are parallel to the P_{\perp} direction. The P_{\parallel} mode is now more favorably reflected back to the cavity. This causes the P_{\parallel} mode to remain strong, but the P_{\perp} mode is substantially suppressed, and therefore the polarization ratio is greatly enhanced. The polarization locking is better illustrated in Fig. 8, which shows the polarization ratio of the strong to the weak mode vs. the injection current with the 100 nm period SWTG. When there is no feedback, the polarization ratio of the output light has a maximum value of 20:1. However, with the SWTG in place, this ratio is greater than 100:1 for both mode switching and mode enhancement over most of the range of injection current. The maximum polarization ratio is about 200:1, and is observed for mode enhancement. For injection currents well above threshold, it is believed that higher order transverse modes begin to emerge, reducing the polarization ratio of the output light. Furthermore, because the SWTG increases the effective reflectivity of the output window, it lowers the threshold current in both mode switching and mode enhancement.

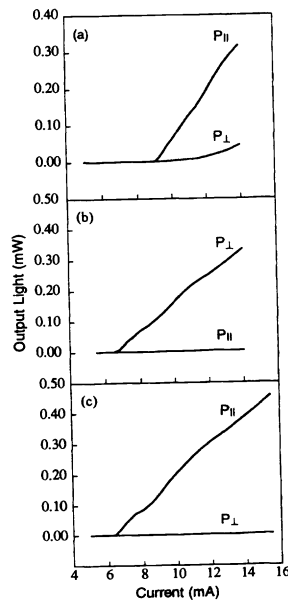


Fig. 7 Light output of a VCSEL vs. injection current (a) without feedback, (b) with SWTG grating fingers parallel to P_{\parallel} and feedback in P_{\perp} direction, (c) with SWTG grating fingers perpendicular to P_{\parallel} and feedback in P_{\parallel} direction. Grating period is 100 nm.

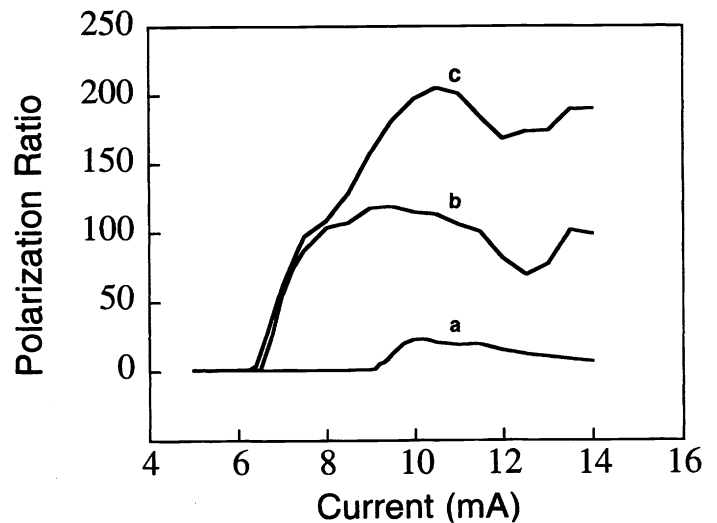


Fig. 8. Polarization ratio vs. injection current (a) without feedback, (b) with SWTG fingers parallel to P_{\parallel} and feedback in P_{\perp} direction, (c) with SWTG grating fingers perpendicular to P_{\parallel} and feedback in P_{\parallel} direction. Grating period is 100 nm.

Polarization mode switching and enhancement are also observed for grating periods ranging from 150 nm to 400 nm, although the effects of mode locking and switching are poor, due to comparable reflectances for the TE and TM modes. For the 450 nm period SWTG, the intra-cavity polarization ratio is observed to be greater than 300:1, which is caused by the near total reflectance of the TM mode at the SWTG. However, this high reflectance also prevents the enhanced light from passing through the SWTG, leading to a low extra-cavity power output for that mode. For periods greater than 500 nm, diffraction effects start to become significant, reducing the coherency and polarization ratio of the light transmitted through the SWTG.

4. TERA-HERTZ FREQUENCY TUNABLE VCSELS

Ultra-high frequency laser pulses play a very important role in many areas of science and engineering. They can be generated directly in two ways: gain switching and mode-locking. The frequency in the gain switching method is intrinsically limited by the carrier relaxation frequency [19]. The frequency in the mode-locking method is determined by the laser cavity length. Currently, the highest frequency demonstrated is 130 GHz for gain switching lasers [20] and 350 GHz [21] for mode-locked lasers; both using edge emitting lasers.

VCSELS, which have a cavity length much shorter than edge emitting lasers, have been used to achieve 6 GHz polarization switching oscillation [22]. In polarization switching, a partially reflecting mirror is placed outside a VCSEL output window, forming an external cavity; and a quarter-wave plate is placed between the VCSEL and the mirror, with the fast axis aligned 45° to the polarization direction. Illustrated in Fig. 9, as linearly polarized light (e.g. $P_{||}$) from the VCSEL passes through the quarter-wave plate, it is converted to, say, right-hand circularly polarized (RHCP) light. The RHCP light is then converted to left-hand circularly polarized (LHCP) light as it reflects off the partial reflector. The LHCP light passes again through the quarter-wave plate and is converted back to linearly polarized light, except at an angle of 90° relative to the initial polarization (i.e. in the P_{\perp} direction). The polarized light is injected back into the VCSEL and switches the polarization of the strong mode from $P_{||}$ to the P_{\perp} polarization direction. The repetition of this cycle leads to an oscillation of the polarization state of the VCSEL at a frequency of $f = c/(4l)$, where c is the speed of light and l is the external cavity length (optical distance from the outer surface of the partial mirror to the outer end mirror of the VCSEL). This frequency corresponds to a period of twice the round trip time of light in the cavity. However, oscillation frequencies higher than 10 GHz are difficult to obtain, since the minimum cavity length is limited by bulky optics, namely the thick quarter-wave plate.

To increase the oscillation frequency of polarization switching VCSELS beyond the 10 GHz range, it has been suggested that a conventional quarter-wave plate should be replaced by a quarter-wave plate made of an α -Si SWTG [23]. By using a SWTG wave plate with a phase retardation of 90° in place of the conventional quarter-wave plate, the cavity length can be significantly reduced, corresponding to a much higher switching frequency. Theoretically, if the cavity length can be reduced to 7.5 μm , a tunable switching frequency of 10 THz can be expected (Fig. 10).

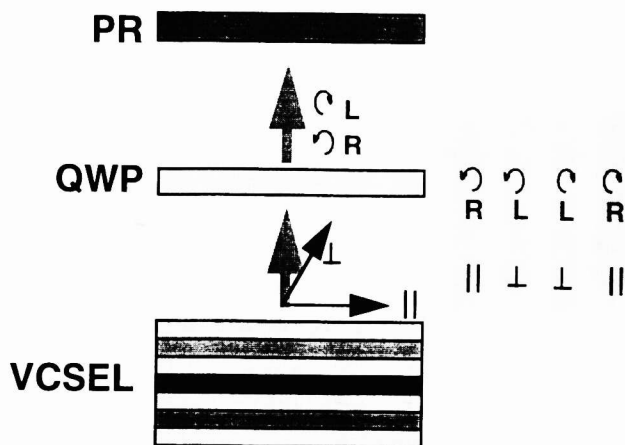


Fig. 9 Polarization switching VCSEL with partial reflector (PR) and quarter-wave plate (QWP). Polarized light (\parallel) is converted to right-hand circular polarization (R) by QWP, reflected back in left-hand circular polarization (L) by PR, and then switched to orthogonal polarization (\perp) by QWP. Injection of polarized light back into VCSEL switches the lasing polarization.

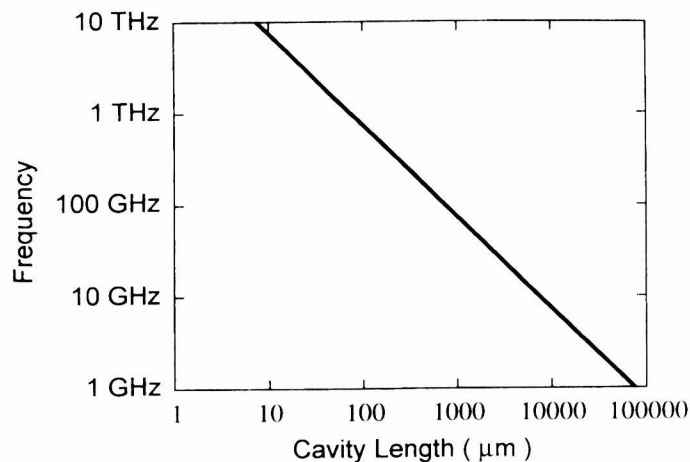


Fig. 10 Polarization switching frequency vs. inverse cavity length when conventional quarter-wave plate is placed between VCSEL and partial reflector. Period of switching is equal to two round trip times for light in the external cavity.

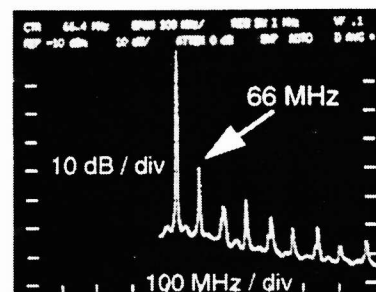
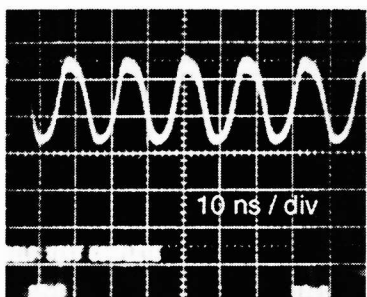


Fig. 11 Wave form and frequency spectrum of VCSEL output showing polarization switching. The external cavity length is 114 cm.

A conventional quarter-wave plate was used to construct a polarization switching VCSEL. The output light, after passing through the partial reflector, was converted back to linearly polarized light outside the cavity using another quarter-wave plate, and was detected using a linear polarizer and an avalanche photodiode. The switching was displayed on an oscilloscope and a spectrum analyzer (Fig. 11). In this setup, modulation depths of up to 90% were obtained at 66 MHz, and switching frequencies between 50 and 1.6 GHz were measured. The oscillation frequency was found to vary with the cavity length. Switching was obtained for all drive currents, but optimum results were obtained near the threshold current, which is 9 mA for the 20 μm VCSEL. Also, tilting of the quarter-wave plate in the cavity, simulating imperfect phase retardation, was shown to have little effect on the polarization switching. This indicates that a wave plate does not need to have a perfect 90° phase retardation. Rotation of the quarter-wave plate by a few degrees also had little effect on the overall polarization switching, although it did produce a split in the fundamental switching frequency. Currently, we are investigating the oscillation at a higher frequency and frequency tunability by mounting the SWTG waveplate and the partial reflector on a micro-actuator. Finally, we recently observed that even without a quarterwave plate, a VCSEL can still oscillates, but at a frequency corresponding to a single round trip and with a linear polarization [24].

5. OTHER APPLICATIONS OF SWTGS

Another application of SWTGs is to place the SWTG narrow band filter in front of a VCSEL. The band filter tunes the VCSEL's lasing wavelength at its resonance reflection wavelength, offering a unique way to generate multiple frequencies needed for wavelength division multiplexing (WDM). Our study for such application is in progress.

6. ACKNOWLEDGMENTS

The author greatly appreciates W.Y Deng for his contribution in developing RMET simulation program and in fabricating and measuring parts of the SWTGs. The work was supported in part by ONR (Dr. Y.S. Park) and NSF (Dr. D. Crawford).

7. REFERENCES

1. S. Y. Chou, and W. Y. Deng, *Appl. Phys. Lett.*, **67**(6), 742-744, 1995.
2. S.J. Schablitsky, Lei Zhuang, Rick C. Shi, and S. Y. Chou, *Appl. Phys. Lett.*, **69**(1), pp 7-9, 1996
3. S.Y. Chou, S. J. Schablitsky, and L. Zhuang, *J. Vac. Sci. and Tech. B* Nov/Dec, 1997.
4. M. Born and E. Wolf, *Principles of Optics*, 6th edition, p. 705, (Pergamon Press, New York, 1980).
5. W. Deng and S. Y. Chou (unpublished)
6. S.S. Wang and R. Magnuson, *Appl. Opt.* **34**, 14 (1995)
7. A. Sharon, D. Rosenblatt, and A.A. Friesem, *Appl. Phys. Lett.* **69**, 4154 (1996)
8. L. H. Cescato, Ekkehart Glutch, and N. Striebl, *Applied Optics* **29**, 3266 (1990).
9. R. C. Enger and S. K. Case, *Applied Optics* **22**, 3220 (1983).
10. D. C. Flanders, *Appl. Phys. Lett.* **42**, 492 (1983).
11. S. Y. Chou, P. R. Krauss, and P. J. Renstrom, *Appl. Phys. Lett.* **67**(21), 3114 (1995), and *Science*, **272**, 85 (1996).
12. W. Wu and S. Y. Chou, unpublished.
13. M. Shimizu, F. Koyama, and K. Iga, *Jpn. J. of Appl. Phys.* **27**, 1774 (1988)
14. K. Choquette and R. Leibenguth, *IEEE Photonics Technol. Lett.* **6**, 40 (1994)
15. T. Yoshikawa, H. Kosaka, K. Kurihara, M. Kajita, Y. Sugimoto, and K. Kasahara, *Appl. Phys. Lett.* **66**, 908 (1995)
16. T. Mukaihara, F. Koyama, and K. Iga, *IEEE Photonics Technol. Lett.* **5**, 133 (1993)
17. D. Vakhshoori, *Appl. Phys. Lett.* **65**, 259 (1994)
18. T. Mukaihara, N. Ohnoki, Y. Hayashi, N. Hatori, and F. Koyama, *IEEE J. Quantum Elect.* **1**, 667 (1995)
19. K. Y. Lau, *Appl. Phys. Lett.* **52**, 257 (1988).
20. Jian Wang and H. Schweizer, *IEEE J. Quantum Electr.* **2:3**, 566 (1996).
21. Y. K. Chen, M. C. Wu, T. Tanbun-Ek, R. A. Logan, and M. A. Chin, *Appl. Phys. Lett.* **58**, 1253 (1991).
22. S. Jiang, Z. Pan, M. Dagenais, R. A. Morgan, and K. Kojima, *Appl. Phys. Lett.* **63**, 3545 (1993).
23. S.Y. Chou, unpublished, 1995.
24. J. Wang and S.Y. Chou, unpublished, 1997.